A Covalent Modification of $NADP^+$ Revealed by the Atomic Resolution Structure of FprA, a *Mycobacterium tuberculosis* Oxidoreductase[†,‡]

Roberto T. Bossi,[§,||] Alessandro Aliverti,[⊥] Debora Raimondi,[⊥] Federico Fischer,[⊥] Giuliana Zanetti,[⊥] Davide Ferrari,[#] Nora Tahallah,[£] Claudia S. Maier,[£] Albert J. R. Heck,[£] Menico Rizzi,[§,||] and Andrea Mattevi*[,§]

Dipartimento di Genetica e Microbiologia, Università di Pavia, Pavia, Italy, DISCAFF, Università del Piemonte Orientale "Amedeo Avogadro", Novara, Italy, Dipartimento di Fisiologia e Biochimica Generali, Università degli Studi di Milano, Milano, Italy, Dipartimento di Biochimica e Biologia Molecolare, Università di Parma, Parma, Italy, and Department of Biomolecular Mass Spectrometry, Bijvoet Center for Biomolecular Research and Utrecht Institute for Pharmaceutical Sciences, Utrecht University, Utrecht, The Netherlands

Received March 22, 2002; Revised Manuscript Received May 14, 2002

ABSTRACT: FprA is a mycobacterial oxidoreductase that catalyzes the transfer of reducing equivalents from NADPH to a protein acceptor. We determined the atomic resolution structure of FprA in the oxidized (1.05 Å resolution) and NADPH-reduced (1.25 Å resolution) forms. The comparison of these FprA structures with that of bovine adrenodoxin reductase showed no significant overall differences. Hence, these enzymes, which belong to the structural family of the disulfide oxidoreductases, are structurally conserved in very distant organisms such as mycobacteria and mammals. Despite the conservation of the overall fold, the details of the active site of FprA show some peculiar features. In the oxidized enzyme complex, the bound $NADP^+$ exhibits a covalent modification, which has been identified as an oxygen atom linked through a carbonylic bond to the reactive C4 atom of the nicotinamide ring. Mass spectrometry has confirmed this assignment. This $NADP^+$ derivative is likely to form by oxidation of the $NADP^+$ adduct resulting from nucleophilic attack by an active-site water molecule. A Glu-His pair is well positioned to activate the attacking water through a mechanism analogous to that of the catalytic triad in serine proteases. The $NADP^+$ nicotinamide ring exhibits the unusual cis conformation, which may favor derivative formation. The physiological significance of this reaction is presently unknown. However, it could assist with drug-design studies in that the modified $NADP^+$ could serve as a lead compound for the development of specific inhibitors.

Tuberculosis is still a major cause of mortality in both developing and industrialized countries. It kills about 3 million people every year, and its rate is increasing (*1*). Among the main factors involved are the high resilience of mycobacteria, poor compliance of patients to treatments, which can result in drug resistant strains, and the HIV epidemic. The picture emerges that, despite a vaccine and effective drugs are available, new antitubercular agents and therapies are needed. With this in mind, a structural genomics project targeting *Mycobacterium tuberculosis* proteins has been undertaken through a worldwide consortium approach (*2*).

We have investigated FprA, a *M. tuberculosis* flavoenzyme encoded by gene Rv3106 of the H37Rv strain of the pathogen (*3*). This 50 kDa enzyme is able to take two reducing equivalents from NADPH and transfer them to a yet-unidentified protein acceptor, via the protein-bound FAD cofactor (*4*). Plant ferredoxin, bovine adrenodoxin, and *Mycobacterium smegmatis* 7Fe ferredoxin can all function as in vitro electron acceptors. Although the physiological role of FprA is still unclear, insights can be derived from its primary structure. A BLAST search (*5*) of FprA sequence against the database retrieves, among the highest score proteins, mammalian adrenodoxin reductase (AR)[1] and the yeast protein Arh1p, displaying 41% and 30% sequence identity, respectively (Figure 1). The yeast homologue Arh1p acts via a ferredoxin and is crucial for iron homeostasis and in vivo assembly of Fe/S proteins (*6*). Inactivation of the gene coding Arh1p has been shown to be lethal (*7*). Mammalian AR is part of steroid and vitamin D biosynthesis. It is a mitochondrial flavoenzyme, which transfers electrons from NADPH to cytochrome P450 through the [2Fe-2S]-

[†] This work was supported by grants from the Ministero della Università e Ricerca Scientifica e Tecnologica ("Biologia strutturale e dinamica di proteine redox" and "Caratterizzazione funzionale, strutturale e genetica della glutammil-tRNA riduttasi di *M. tuberculosis*"), the European Union ("Quality of Life and Management of Living Resources", Contract QLK2-2000-01761), and the Netherlands Organization for Scientific Research (#99508).

[‡] Data deposition: coordinates of *M. tuberculosis* FprA structures in the oxidized and reduced form have been deposited in the Protein Data Bank (*39*) with accession codes 1LQT and 1LQU, respectively.

* Corresponding author. Address: Andrea Mattevi, Dipartimento di Genetica e Microbiologia, Università di Pavia, via Abbiategrasso 207, 27100 Pavia, Italy. Phone: +39-0382-505560. Fax: +39-0382-528496. E-mail: mattevi@ipvgen.unipv.it.

[§] Università di Pavia.

[||] Università del Piemonte Orientale "Amedeo Avogadro".

[⊥] Università degli Studi di Milano.

[#] Università di Parma.

[£] Utrecht University.

[1] Abbreviations: AR, adrenodoxin reductase; NADPO, $NADP^+$ derivative; rmsd, root-mean-square deviation; ESI-MS, electrospray ionization mass spectrometry; CID, collisionally induced dissociation.

10.1021/bi025858a CCC: $22.00
Published on Web 06/19/2002

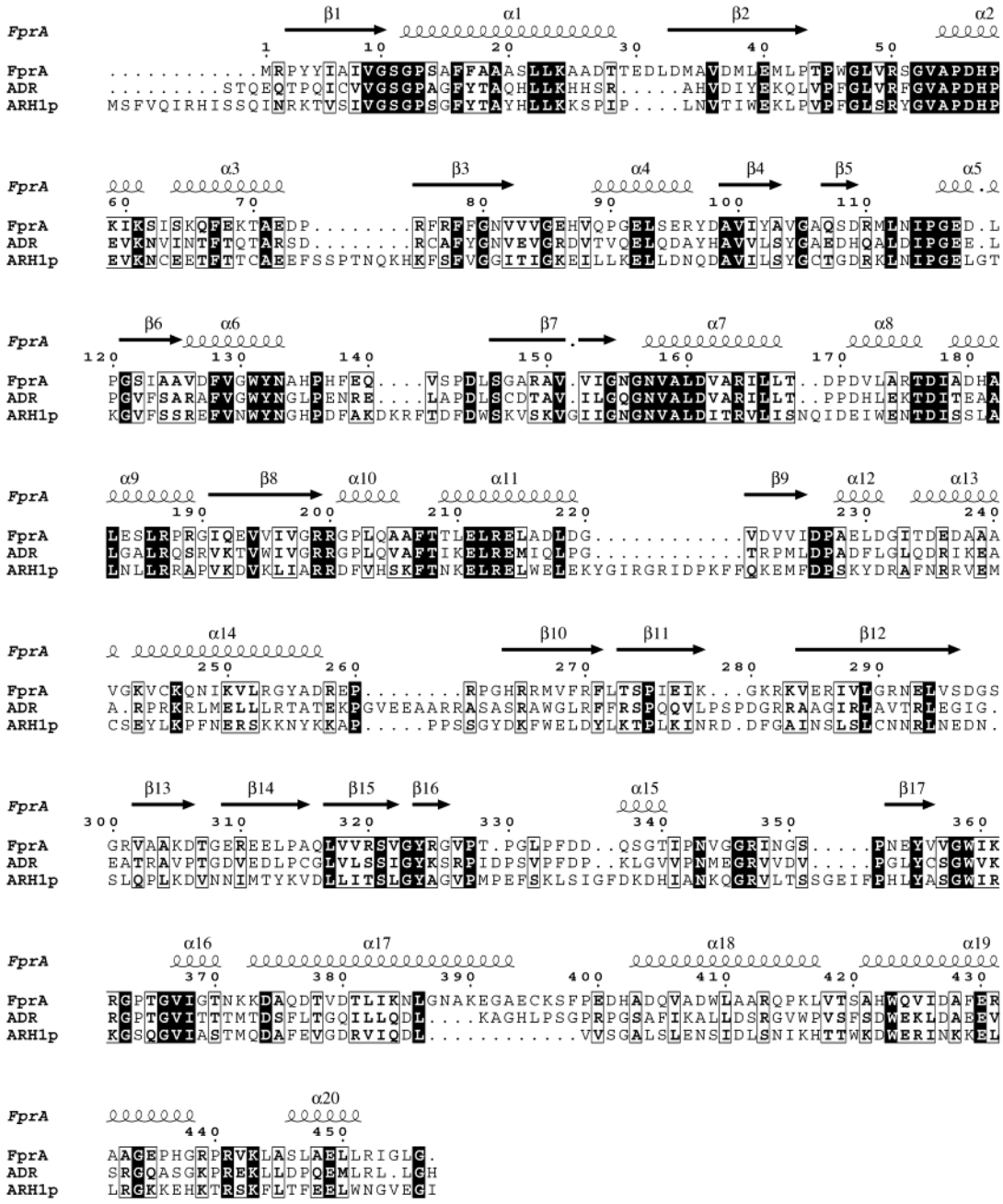

FIGURE 1: Sequence alignment of *M. tuberculosis* FprA, bovine AR, and yeast Arh1p as calculated with CLUSTALW (*40*). The secondary structure elements are for the structure of FprA.

protein adrenodoxin (*8*−*10*). All these data suggest a relevant role of FprA, possibly in Fe metabolism or in cytochrome P450-dependent reactions. While the former process is known to be crucial for mycobacterial infection (*11*), the latter should also be important, since *M. tuberculosis* genome contains 22 genes coding putative cytochrome P450 proteins (*3*).

Recently, the structure of bovine AR in complex with $NADP^+$, NADPH and adrenodoxin has been solved (*12*−*14*). These structures revealed the binding mode of NADP(H) and FAD and the mainly polar interaction between AR and adrenodoxin. Here, we present the crystal structure of FprA in two redox states, obtained by cocrystallization of the oxidized enzyme with $NADP^+$ (FprA:NADPO) and by soaking the crystals in a NADPH-containing solution, which yielded the complex between the reduced enzyme and NADPH ($FprA_{red}$:NADPH). The very high resolution of the diffraction data allowed us to analyze in detail these structures. In the oxidized enzyme, a novel covalent derivative of the pyridine nucleotide has been found (abbreviated as NADPO; Figure 2) and characterized by mass spectrometry.

EXPERIMENTAL PROCEDURES

Sample Preparation and Crystallization. Recombinant FprA was overexpressed and purified as described (*4*). FprA was crystallized at 4 °C by the vapor diffusion method in both hanging and sitting drops. Before crystallization, the enzyme was incubated for about 1 hour in a solution containing $NADP^+$. The enzyme solution contained 25 mg FprA/ml, 10 mM Hepes/KOH pH 7.0, 10% (v/v) glycerol, 5 mM dithiothreitol, and 0.65 mM $NADP^+$. The well solution

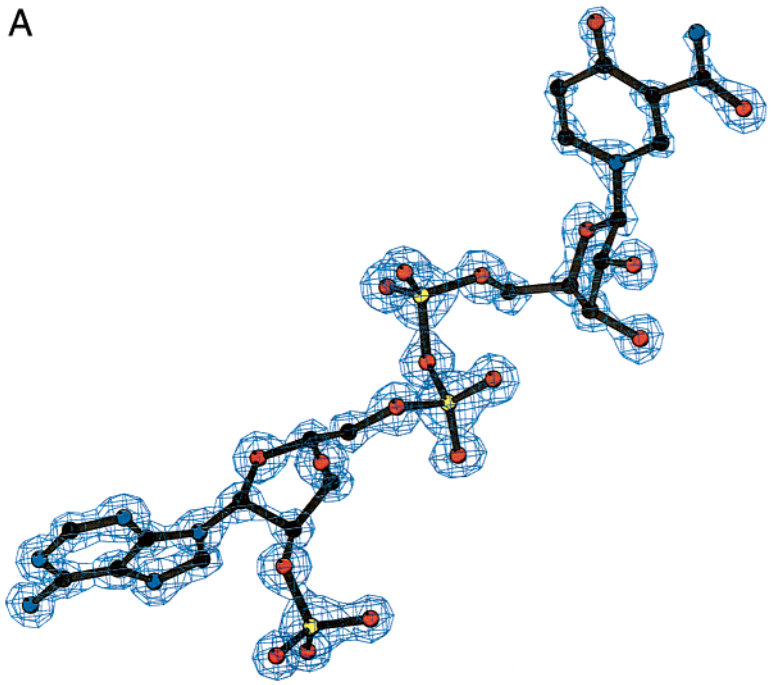

Bond Distances	Monomer A (Å)	Monomer B (Å)
N1-C2	1.41	1.37
C2-C3	1.35	1.37
C3-C4	1.40	1.45
C4-O4	1.27	1.23
C4-C5	1.47	1.45
C5-C6	1.41	1.40
N1-C6	1.38	1.38
C3-C7	1.54	1.52
C7-O7	1.25	1.25
C7-N7	1.31	1.30

FIGURE 2: Crystallographic data for identification of the modified $NADP^+$. (A) The final 2Fo−Fc electron density map of the covalently modified $NADP^+$ found in the FprA:NADPO complex. The resolution is 1.05 Å. The contour level is 2σ. Carbon atoms are in black, oxygen in red, nitrogen in blue, and phosphorus in yellow. (B) Atomic numbering and crystallographic bond distances of the nicotinamide ring of the $NADP^+$ derivative.

consisted of 30% (w/v) poly(ethylene glycol) 4000, 0.1 M sodium citrate pH 5.6, and 0.2 M ammonium acetate. Crystals grow in approximately 1 week, reaching a maximum size of 0.1 × 0.1 × 1.0 mm^3. They belong to space group $P2_12_12_1$ with unit cell axes a = 69.3 Å, b = 89.2 Å, and c = 160.9 Å.

Single-Crystal Microspectrophotometry and NADPH Soaking. UV−visible spectra on FprA were recorded on single crystals at room temperature, using a Zeiss MpM800 microspectrophotometer (*15*). Crystals were harvested in a stabilizing solution containing 32% (w/v) poly(ethylene glycol) 4000, 0.1 M sodium citrate pH 5.6, 0.2 M ammonium acetate, and 0.65 mM $NADP^+$ and then placed in a quartz cell with a crystal face orthogonal to the incident light beam. Spectra were measured at different times before and after soaking under aerobic conditions in a stabilizing solution containing 10 mM NADPH instead of $NADP^+$. The microspectrophotometric analysis indicated that FprA crystals are reduced after about 30 min of soaking in NADPH. This soaking protocol was used for the structure determination of the $FprA_{red}$:NADPH complex.

Data Collection and Processing. For data collection, FprA crystals were cryoprotected in a solution consisting of 30% (w/v) poly(ethylene glycol) 4000, 0.1 M sodium citrate pH 5.6, 0.2 M ammonium acetate, 20% (v/v) glycerol and 0.65 mM $NADP^+$, and then flash-cooled in a 100 K nitrogen stream. For the NADPH-soaked structure, the cryoprotecting solution contained 10 mM NADPH instead of 0.65 mM $NADP^+$. Data were collected at the BW7B beamline of the EMBL/DESY Outstation (Hamburg) using a MAR image plate detector. Data integration was performed by MOSFLM (*16*), whereas merging and scaling were made using the CCP4 program suite (*17*). A summary of the data collection statistics is reported in Table 1.

Table 1: Data Collection and Refinement Statistics

	FprA:NADPO	$FprA_{red}$:NADPH
space group	$P2_12_12_1$	$P2_12_12_1$
a,b,c (Å)	69.3, 89.2, 160.9	69.5, 89.5, 161.6
resolution limit (Å)	1.05	1.25
total observations	1 170 509	877 990
unique reflections	440 216	275 836
overall completeness (%)	95.8	98.1
completeness outermost shell (%)	95.4	98.1
overall I/σ(I)	5.1	9.1
$I/\sigma(I)$ outermost shell	1.6	2.5
R_{sym} (%)[a]	7.1	5.3
R-factor (%)[b]	13.4	12.5
R-free (%)[b]	15.3	14.2
rmsd bond length (Å)[c]	0.015	0.014
rmsd bond angle (deg)[c]	1.747	1.666
Ramachandran plot (%)[d] most favored/additional	93.9/5.6	93.8/5.6
asymmetric unit[e]		
protein	7104	7006
FAD	106	106
NADP	98	96
water	1864	1422
acetate	44	44

[a] $R_{sym} = \Sigma_{hkl,i}|I_{hkl,i} - \langle I_{hkl}\rangle|/\Sigma_{hkl,i}\ I_{hkl,i}$. [b] R-factor $= \sum||F_o| - |F_c||/\sum|F_o|$, where the working and free R-factors are calculated using the working and free reflection sets, respectively. The free reflections (0.5% of the unique reflections) were held aside throughout the refinement and included in the last cycle only. [c] Calculated with Refmac5 (*22*). [d] As classified by PROCHECK (*24*). [e] Number of atoms in the asymmetric unit. Hydrogen atoms are not included. The FprA subunit consists of 456 amino acids. The only missing amino acids are, in FprA:NADPO, Pro260, Pro399, and Glu400 in monomer A and Glu400 in monomer B, and, in $FprA_{red}$:NADPH, Pro260 and Glu400 in monomer A and Glu400 in monomer B. Alternate conformations were modeled for 35 residues in FprA:NADPO and 16 residues in $FprA_{red}$:NADPH.

Structure Determination and Refinement. For structure determination, data of the FprA:NADPO complex obtained

by cocrystallization with $NADP^+$ were used. The structure was solved through molecular replacement using the structure of bovine adrenodoxin reductase (PDB entry 1E1L; *13*) as the search model and the program BEAST (*18*). Employment of this program improved the clarity of the solutions found in the molecular replacement calculations, indicating the presence of a FprA dimer in the asymmetric unit. The 2-fold noncrystallographic symmetry was exploited to improve the model phases by density modification through the program DM (*19*). Native data up to 1.9 Å resolution and DM phases were used to automatically build the model by the ARP/wARP package (*20*). For the success of the autobuilding procedure, it was essential to down-weight the model phases in the phase combination steps of the DM density modification calculations (for a description of the protocol, see ref *21*). A total of 900 residues (out of 912) were automatically positioned in the electron density using ARP/wARP (*20*). This structure was further refined by Refmac5 using standard protocols (*22*). All measured reflections up to 1.05 Å resolution were used. Individual anisotropic displacement parameters and hydrogen atoms at their idealized positions have been introduced. Model building was performed with O (*23*). No restraints were applied to both FAD and $NADP^+$ to allow detection of any unusual stereochemical feature in these ligands. Ordered water molecules were generated with the program ARP (*20*) using the criteria that the peaks in 2Fo−Fc and Fo−Fc maps had to be higher than 1.25 and 3.0 σ, respectively, and that the water molecules had to be within H-bond distances from a protein or solvent atom. Except for the last refinement cycle, 0.5% of unique reflections were excluded from calculations to perform R-free validation. The model of FprA:NADPO provided the starting coordinates for refinement of the $FprA_{red}$:NADPH structure, performed at 1.25 Å resolution. Also for this structure, individual anisotropic displacement parameters and hydrogen atoms at their idealized positions have been introduced. Refinement statistics are summarized in Table 1.

Structure analysis was done using O (*23*), PROCHECK (*24*), ACONIO (*25*), and programs from the CCP4 package (*17*). Figures were produced by MOLSCRIPT (*26*), BOBSCRIPT (*27*), and LIGPLOT (*28*).

Mass Spectrometry. All mass spectrometry experiments were performed in the positive ion mode. The mass analyses were carried out on a LC-T orthogonal time-of-flight (ToF) instrument equipped with a Z-spray nanoelectrospray ion source (Micromass, Manchester, UK). Gold-coated borosilicate glass capillaries were used for sample introduction and prepared as described previously (*29*). The capillary and cone voltages were optimized for stable spraying conditions. The source temperature was set to 60 °C. For optimal detection of the noncovalently associated species, collisional cooling conditions were employed as described previously (*29*). Deconvolution of conventional ESI mass spectra of protein samples was performed by maximum entropy processing using the MaxEnt program incorporated in the Micromass MassLynx software.

For mass spectrometry analysis, the protein stock solution (25 mg FprA/ml, 10 mM Hepes/KOH pH 7.0, 10% glycerol and 0.65 mM $NADP^+$) was diluted directly into 50 mM ammonium acetate solution (pH 6.8). For determining the molecular mass of the apoprotein, denaturing conditions were used by diluting the protein stock solution into 0.7% formic acid. Sample concentrations were adjusted to 3−25 μM monomer concentration.

A Q-ToF mass spectrometer also fitted with a Z-spray nanoelectrospray ion source (Micromass, Manchester, U.K.) was used for CIS MS/MS experiments. After optimizing capillary voltage and cone voltage settings, the resolution of the mass-analyzing quadrupole was set so that the full isotopic envelope of the selected precursor ion was transmitted. Argon was used as collision gas. The collision offset potentials were typically set to 20−75 V. The calculated monoisotopic masses M_{th} based on the respective chemical formulas are 744.08 u for $NADP^+$ ($C_{21}H_{29}O_{17}N_7P_3$), 759.08 u for the $NADP^+$ derivative ($C_{21}H_{28}O_{18}N_7P_3$), and 785.56 u for FAD ($C_{27}H_{33}O_{15}N_9P_2$).

RESULTS AND DISCUSSION

Crystallographic Analysis. Growth of FprA crystals was possible only by cocrystallization with $NADP^+$, while crystals of the free enzyme were never obtained. The structure of oxidized FprA has been solved at 1.05 Å resolution in complex with $NADP^+$ (FprA:NADPO). Structure determination has been performed through molecular replacement, using bovine AR (*12*) as search model. Employment of a maximum likelihood scoring function (*18*) in molecular replacement greatly facilitated structure solution. Soaking in a NADPH-containing mother liquor led to reduction of the crystalline protein ($FprA_{red}$:NADPH complex). We have collected data up to 1.25 Å resolution on a NADPH-soaked crystal and solved this second structure using the atomic coordinates of FprA:NADPO. The asymmetric unit of FprA crystals contains a protein dimer (2 × 50 kDa) with the two subunits related by a noncrystallographic 2-fold axis (Figure 3a). The electron density (Figure 2a) allowed the positioning of the FAD cofactor, of the NADP ligand, and of nearly all 456 residues of each FprA monomer (Table 1). The refined models have an *R*-factor of 13.4% (*R*-free 15.3%) for FprA:NADPO and 12.5% (*R*-free 14.2%) for $FprA_{red}$:NADPH (Table 1).

Overall Structure. The FprA monomer consists of two α/β domains with similar topologies (Figure 3b). The FAD-binding domain consists of the N- and C-terminal regions of the enzyme (residues 2−106 and 327−456), whereas the central part of the polypeptide chain (residues 110−323) forms the NADP-binding domain; a small two-stranded β-sheet (residues 107−109 and 324−326) links the two domains. This overall architecture is common to the proteins belonging to the structural family of glutathione reductase (*30, 31*), of which FprA is a member. Both domains of FprA exibit a Rossmann fold topology (*32*), but some variations are present in this scaffold. The FAD-binding domain has a central five-stranded parallel β-sheet surrounded on both sides by α-helices. Although within this family of proteins the crossover between strand 3 and strand 4 is typically an antiparallel β-sheet (the so-called β-meander) (*30*), in FprA this is replaced by an α-helix (helix 89−96). A six-stranded central β-sheet is present in the NADP-binding domain, flanked on one side by α-helices and on the other side by the β-meander.

In the X-ray structure, FprA is present as a dimer (Figure 3a). The intersubunit interactions are not extensive involving only 5.6% (1138 $Å^2$) of the monomer surface area, suggesting

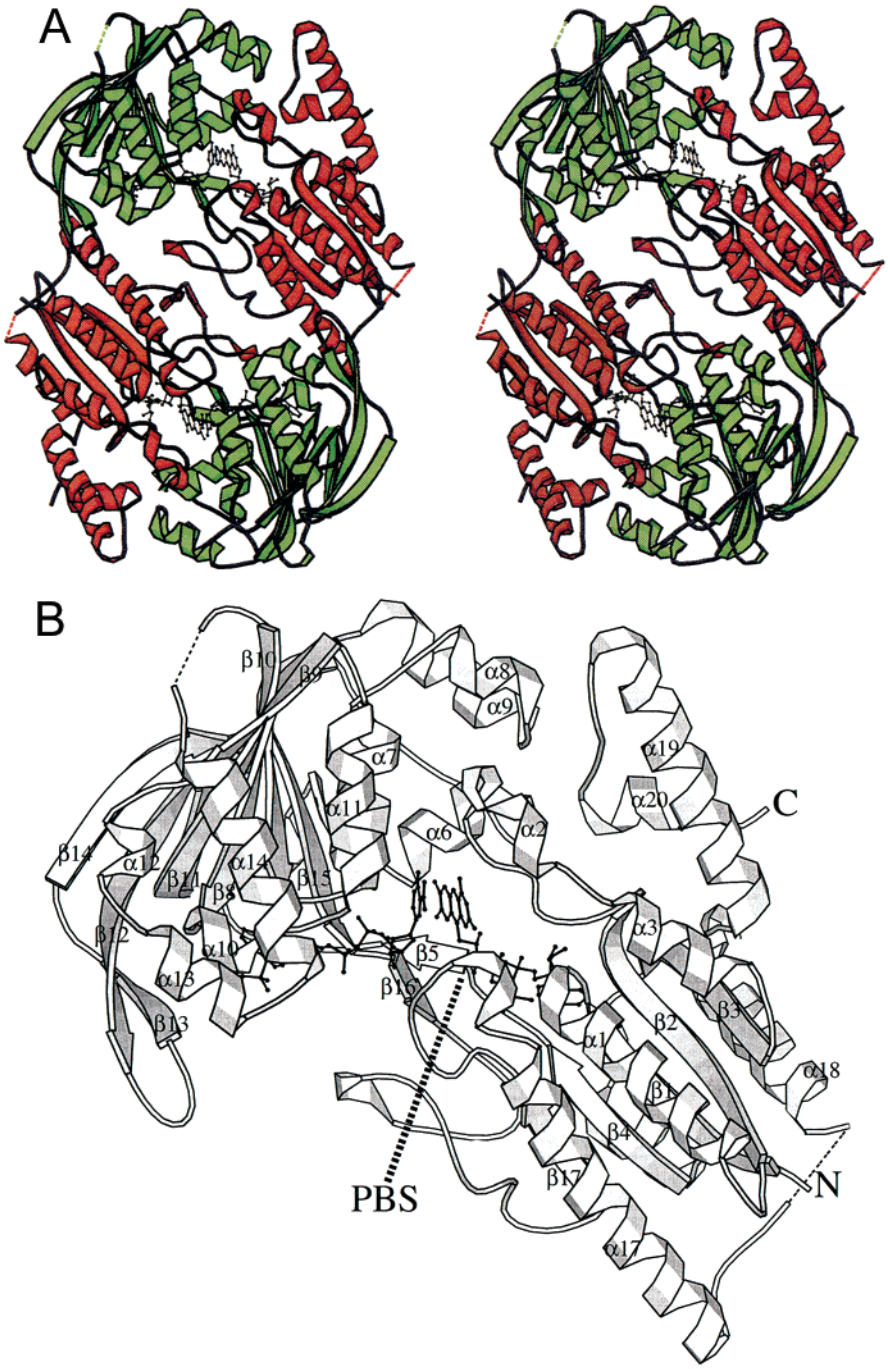

FIGURE 3: Three-dimensional structure of FprA. (A) Stereoview of the FprA dimer. The noncrystallographic 2-fold axis is perpendicular to the plane of the drawing. The FAD-binding domain is in red, while the NADP-binding domain is in green. The FAD cofactor is yellow, and the modified $NADP^+$ ligand is black. The dashed lines connect residues at the borders of disordered regions of the protein. (B) The FprA monomer. Secondary structures are labeled as in Figure 1. The letters "N" and "C" indicate the N-terminal and C-terminal residues, respectively. The putative binding site for the protein partner is labeled as "PBS". It is located in a cleft between the FAD-binding and NADP-binding domains.

that dimerization is probably a result of crystal packing. This notion is supported by gel-filtration studies, which indicate that the enzyme in solution is mainly monomeric (*4*). The two crystallographically independent monomers are virtually identical, with a root-mean-square deviation (rmsd) of 0.83 Å for 3447 atom pairs in FprA:NADPO and 0.89 Å for 3454 pairs in $FprA_{red}$:NADPH.

The interactions between FprA and the prosthetic group (Figure 4a) resemble those typically found for FAD binding within the structural family of glutathione reductase (*32*), with the characteristic N-terminal $\beta\alpha\beta$ unit (residues 3−43) involved in the binding of the cofactor ADP moiety. The isoalloxazine is bound in a planar conformation. The angle between pyrimidine and dimethylbenzene rings is 4°, implying a very small tilting of the flavin. The cofactor pyrimidine ring is partly exposed to the solvent while the dimethylbenzene ring is buried in the flavin-binding site. The N-terminus of α-helix 367−393 interacts with the electronegative N1−

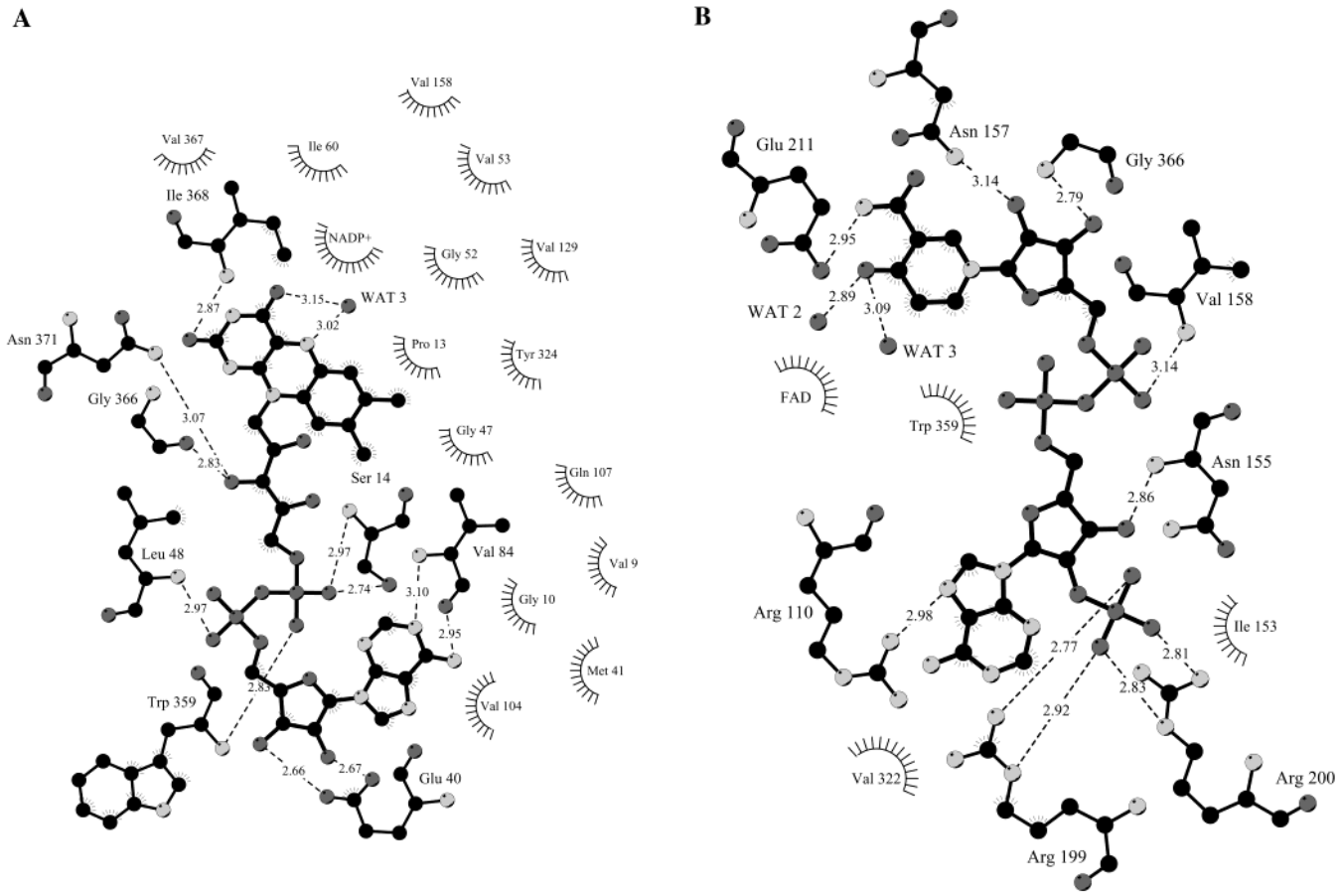

FIGURE 4: Schematic representation of the binding of FAD (A) and modified $NADP^+$ (B) to monomer A of FprA:NADPO. H-bonds are shown as black-broken lines. Distances are in Å. Shading around atoms and residue labels indicates involvement in van der Waals contacts. Atoms are color coded as follows: black, carbon; dark gray, oxygen and phosphorus; light gray, nitrogen.

O2 locus of the flavin and directly binds to O2 with Ile368 N atom. Loop 358−366 covers the active site as a cap, interacting with both the flavin and the NADP ligand.

Comparison with Adrenodoxin Reductase. The structure of AR has been solved in different states (*12*−*14*), namely, in the native form (PDB code 1CJC), cocrystallized with $NADP^+$ (1E1L), soaked with $NADP^+$ or NADPH (1E1K and 1E1M), and in complex with adrenodoxin (1E6E). The overall structures of FprA and AR are highly similar, especially in the FAD-binding domain. Superposition of the FAD-binding domain of FprA (monomer A of FprA:NADPO) onto the equivalent domain of AR results in rmsds below 0.85 Å (164 Cα pairs) for all AR structures, while superposition of the NADP-binding domain produces rmsds below 1.8 Å (212 Cα pairs). However, some differences exist in the domain orientations. This aspect was investigated by calculating the rotation angle required to optimally superimpose the NADP-binding domain of FprA onto that of AR, starting with the FAD-binding domains superimposed. The smallest value (4.5°) resulted from the superposition between FprA and AR cocrystallized with $NADP^+$. The corresponding angle was 6° for AR soaked in NADP(H) and 8.3° for AR in complex with adrenodoxin. This analysis indicated that FprA and AR differ in that FprA domains adopt a slightly more "open" orientation relative to the AR structures.

The binding site for adrenodoxin in AR is formed by a shallow cleft (Figure 3b), which is located between the FAD-binding and NADP-binding domains (*14*). Several charged residues on the cleft surface take part in the interaction with the protein partner. It is noticeable that many of these amino acids are conserved in FprA (Lys24, Arg213, Lys246, Arg362, and Asp374), consistent with the observation that FprA binds bovine adrenodoxin and possesses NADPH−adrenodoxin oxidoreductase activity (*4*). A search of the *M. tuberculosis* genome reveals no genes coding proteins that have clear homology to adrenodoxin. Thus, the similarity between AR and FprA in the binding site is likely to reflect conservation in the electrostatic nature of the interaction with their respective protein partners, which, however, may be structurally dissimilar.

$NADP^+$ Derivative. The NADP ligand binds in an extended conformation in a solvent-accessible position, being in contact with many ordered water molecules (Figures 3 and 4b). As usual for this kind of nucleotide-binding fold (*32*−*34*), the substrate ADP moiety is accommodated within the NADP-binding domain. The nicotinamide ring is bound at the domain interface between the FAD isoalloxazine ring and Asn157 with the substrate amide group H-bonded to the side chain of Glu211. The nicotinamide is essentially parallel to the flavin (Figure 5a) with an angle between the two rings of 9°. The reactive C4 atom of $NADP^+$ is at 3.27 Å from N5 of FAD in monomer A and at 3.31 Å in monomer B. An unexpected feature emerged during refinement was an additional electron density present on the nicotinamide ring of both monomers of FprA:NADPO (Figure 2a). The detailed investigation of the electron density and the environment of

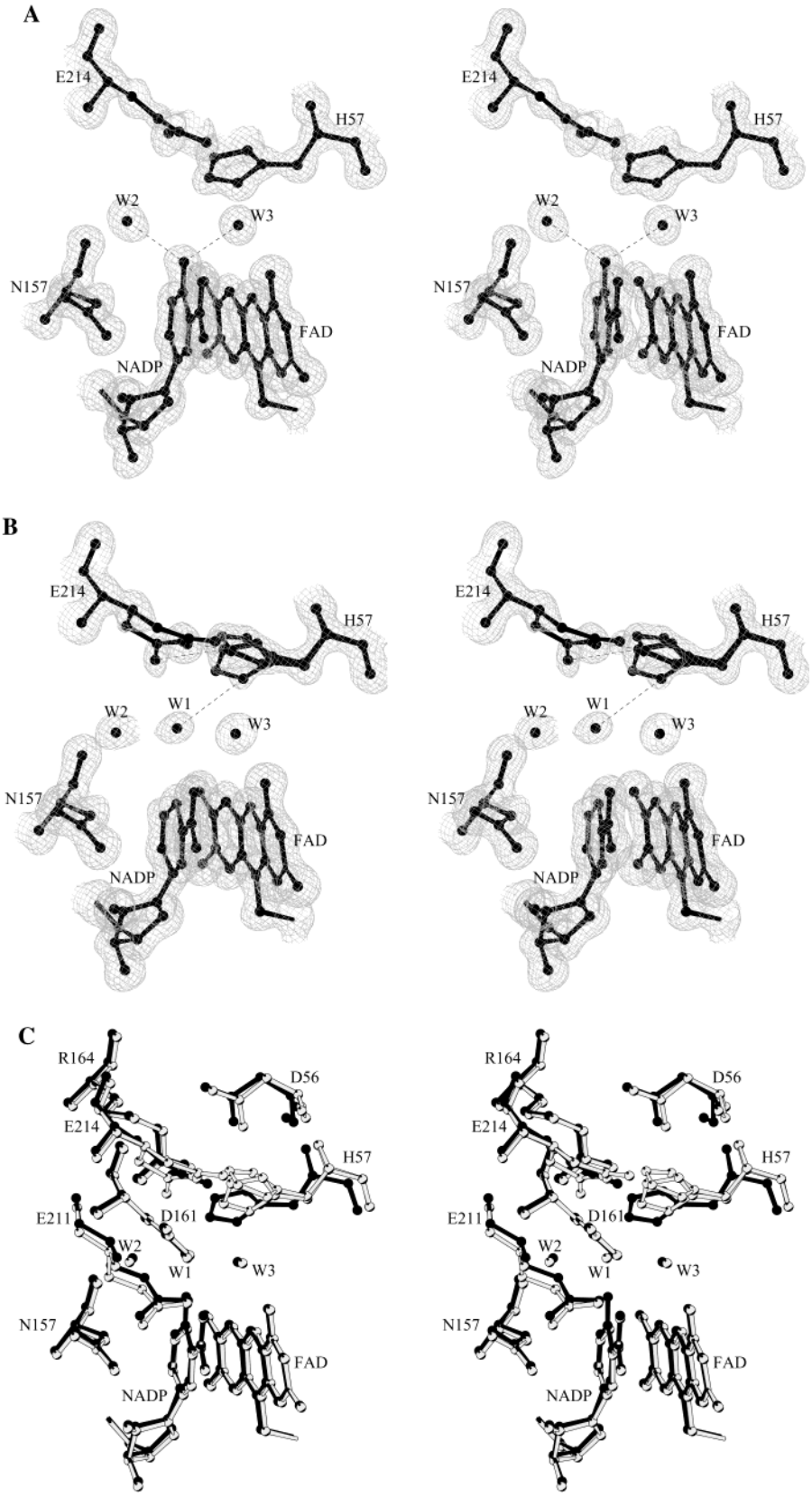

FIGURE 5: Active site of FprA (monomer A). The orientation is the same as that in Figure 3. H-bonds are outlined by dashed lines, and water molecules are labeled by "W". *B*-factor values of the water molecules are W2 = 16.2 Å^2 and W3 = 9.9 Å^2 for FprA:NADPO; W1 = 24.1 Å^2, W2 = 22.0 Å^2 and W3 = 13.4 Å^2 for FprA$_{red}$:NADPH. (A) Stereo diagram of the electron density (contoured at 1σ) of the modified nicotinamide ring and neighboring residues in the FprA:NADPO complex. (B) Stereo diagram of the active site of FprA$_{red}$:NADPH structure. His57 and Glu214 have alternate conformations (see text). (C) Superposition of the active site residues of FprA:NADPO (black) and FprA$_{red}$:NADPH (light gray) structures.

the ligand led us to the conclusion that the additional density represents an extra oxygen atom linked through a carbonylic bond to the C4 atom of NADP$^+$ (Figure 2b). There are many data in support of this interpretation.

(i) The planarity of the nicotinamide ring was assessed by calculating the angle α_N between the planes N1−C2−C6 and C2−C3−C6 and the angle α_C between the planes C2−C3−C6 and C3−C4−C5. These parameters are useful to quantitatively assess the "out-of-plane" position of the N1 and C4 atoms of the ring, respectively (*35*). The resulted values were $\alpha_N = 2.6°$ and $\alpha_C = 0.6°$ for monomer A and $\alpha_N = 0.3°$ and $\alpha_C = 1.5°$ for monomer B. These values indicate that the nicotinamide ring is almost perfectly planar and support the notion that the C4 atom has trigonal planar configuration.

(ii) The position of the extra atom was defined by refining without setting any restraint on distances and angles on $NADP^+$. The result of these calculations was the placement of this atom at 1.27 Å from C4 in monomer A and 1.23 Å in monomer B (Figure 2b). These values are in perfect agreement with the presence of a carbonylic oxygen bound to C4.

(iii) The extra atom is within H-bond distance from two water molecules and the nitrogen atom of the amide moiety of nicotinamide. The latter H-bond is made possible by the cis conformation of the amide of the FprA-bound $NADP^+$ (i.e., the oxygen points toward the ribose, see Figures 2a and 4b).

(iv) The shape of the electron density for the extra atom, contoured at different levels, is in good agreement with it being an oxygen. This assignment could be made thanks to the atomic resolution of the X-ray analysis, which allowed us to distinguish between oxygen and nitrogen atoms for all Asn and Gln amide moieties of the protein. The *B*-factor of the oxygen atom is 16.6 $Å^2$ in monomer A and 11.7 $Å^2$ in monomer B. These values do not differ from the *B*-factors of the other atoms of the nicotinamide ring, implying that the $NADP^+$ derivative is bound with full occupancy to both subunits of the crystalline enzyme.

Taken together, these data strongly indicate that the modified $NADP^+$ is a quinonic compound, as depicted in Figure 2b (this compound has been named NADPO).

The active site of FprA is a highly polar environment, with basic and acidic residues as well as several water molecules. All these elements have ordered conformations and set up an intricate network of hydrogen bonds. In this milieu, a central role is fulfilled by two water molecules, which, in monomer A, have been designated water 2 and water 3 (Figure 5a). They are both H-bonded to the oxygen atom of NADPO, being on different sides of the nicotinamide plane (Figure 5a). They also interact with several active site residues, and water 3 is bound to the N5 and O4 atoms of FAD (Figs. 4a, 5a and 5b).

Characterization by Mass Spectrometry. In electrospray ionization mass spectrometry (ESI-MS), protein molecules are detected as multiply protonated species. Initial mass spectrometry experiments on FprA incubated with $NADP^+$ were performed under pseudophysiological conditions, i.e., in 50 mM ammonium acetate solutions (pH 6.8,) allowing direct observation of functional multicomponent protein complexes (*36*). The mass spectrum displayed an intensive charge state distribution comprising four abundant ions carrying 16−13 protons with the 15-fold protonated ion at *m*/*z* 3405 predominating. To facilitate interpretation, we deconvoluted the conventional ESI mass spectrum to the so-called "zero-charge" mass spectrum, allowing the direct extraction of the molecular mass of the ion species analyzed (Figure 6a). Centroiding of the mass peak of the transformed mass spectrum gave an average mass of 51 040 ± 10 Da, corresponding to the ternary complex consisting of the FprA monomer, FAD, and the $NADP^+$ substrate. Unfortunately, the mass determination was not sufficient to distinguish if $NADP^+$ or its derivative was present.

To obtain the molecular masses of the apoprotein and the individual ligands, we transferred the protein stock solution into 0.7% formic acid. Under these conditions, the protein should denature, and the ligands should be released. The mass spectrum obtained under these denaturing conditions was dramatically different compared to that obtained in near-physiological solutions. ESI mass spectra acquired from denaturing solutions exhibited a broad charge state distribution of highly protonated protein ions located below *m*/*z* 1600. The "zero-charge" mass spectrum obtained after deconvolution is depicted in Figure 6a. The molecular mass of the apo-FprA monomer was 49 477 ± 5 Da, in good agreement with the expected average mass of FprA derived from the gene sequence after adding the residue mass for the initiation methionine (average M_{th} = 49 472.3 Da).

Besides the apoprotein ions, molecular ions at *m*/*z* 744.1, 760.3, and 786.1 were present in the lower *m*/*z* range, indicating the presence of $NADP^+$, the proposed $NADP^+$ derivative, and FAD, respectively. Interestingly, $NADP^+$ is detected as an M^+ ion because of its fixed positive charge in the nicotinamide moiety, whereas the other two cofactors are detected as the commonly observed $[M + H]^+$ ions. Collisionally induced dissociation (CID MS/MS) experiments yield structure-specific fragment ions that allow assessing the compound identity. For example, the CID MS/MS experiments on the selected $[M + H]^+$ ion of FAD at *m*/*z* 786 resulted in three fragment ions at *m*/*z* 136, 348, and 439, representing the adenine, the adenosine 5′-monophosphate, and the riboflavin 5-monophosphate moiety, respectively. Thus, these structure-specific fragment ions unequivocally confirmed the original assignment of the *m*/*z* 786 ion as the molecular ion of FAD. In a similar fashion, we used CID MS/MS to identify the ion at *m*/*z* 760, the proposed molecular ion of NADPO. For this purpose, we compared the fragment ions of the parent ion at *m*/*z* 760 with the fragment ions that resulted from CID MSMS of the parent ion at *m*/*z* 744, the M^+ ion of $NADP^+$. Several structure-specific fragment ions were observed beside fragment ions that originated from low-energy fragmentation pathways, such as the loss of H_3PO_4 (Δ*m* 98 u), HPO_3 (Δ*m* 80 u) and H_2O (Δ*m* 18 u). The structure-specific fragment ions of NADPO are depicted in Figure 6b. The fragment ions at *m*/*z* 136, 330, 508, and 622 were also observed for $NADP^+$, while the fragment ions at *m*/*z* 139, 351, 431, and 625 were specific for the $NADP^+$ derivative. The observation of the fragment ions at *m*/*z* 351 and 139 allowed the assignment of the derivative to the nicotinamide moiety. It is noteworthy that the *m*/*z* values of all observed derivative specific fragment ions were consistent with the covalent modification being due to a carbonylic oxygen. Most importantly, the mass spectrometry analysis unambiguously showed that formation of the covalent adduct occurs in solution and, therefore, it is not an artifact of the crystallization process.

NADPH-Soaked FprA. Soaking of the crystals in a NADPH-containing solution resulted in the reduction of the crystalline enzyme, as indicated by the loss of the crystal

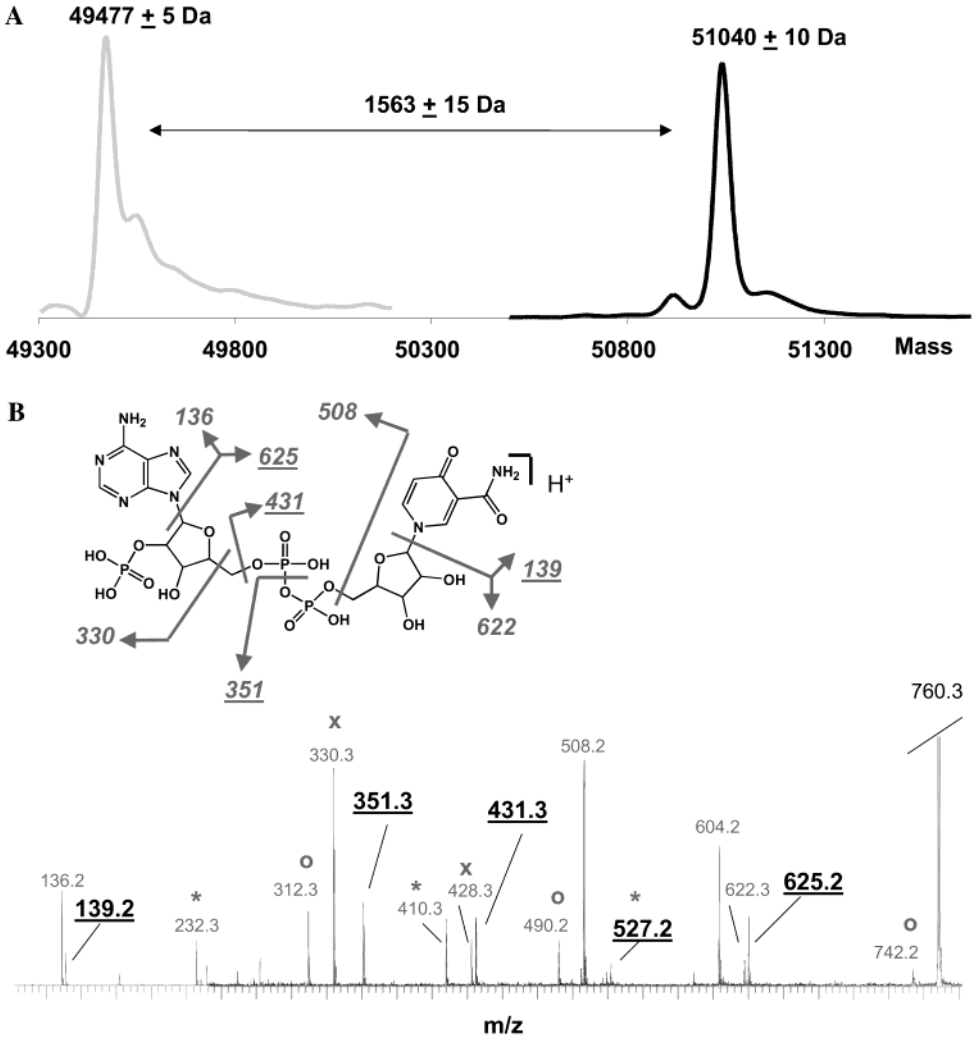

FIGURE 6: (A) Comparison of the deconvoluted mass spectrum obtained for the apoform of FprA (gray line, $M_r = 49\,477 \pm 5$ Da) and the FprA:NADPO holoprotein (black line, $M_r = 51\,040 \pm 10$ Da). (B) Fragment ion spectrum and fragmentation scheme of the $NADP^+$ derivative (MH^+ 760.3). The underlined fragment ions are indicative of the $NADP^+$ derivative. Fragment ions marked with *, x, and o originate from low-energy fragmentation pathways and refer to the loss of H_3PO_4 ($\Delta m = 98$ u), HPO_3 ($\Delta m = 80$ u), and H_2O ($\Delta m = 18$ u), respectively.

yellow color. To investigate the reactivity of the crystalline enzyme, we subjected the crystals to microspectrophotometry analysis (*15*). UV−visible absorption spectra of a FprA crystal are shown in Figure 7. Upon soaking in NADPH under aerobic conditions, the height of the typical absorption peak at 452 nm of the enzyme-bound oxidized cofactor (*4*) decreases, coupled to increased absorption at longer wavelengths. These features suggest that NADPH soaking leads to cofactor reduction, with FAD mainly in the semiquinone one-electron reduced form. In the NADPH-soaked structure, the conformation of the nicotinamide ring deviates from planarity ($\alpha_N = 4.8°$ and $\alpha_C = 7.8°$ for monomer A and $\alpha_N = 5.1°$ and $\alpha_C = 4.8°$ for monomer B). This geometry supports the presence in the crystals of the reduced form of the ligand (*35*), which, therefore, has been modeled as NADPH. This interpretation is in agreement with solution studies, which have shown that aerobic incubation of FprA with excess NADPH leads to accumulation of the neutral semiquinone form of FAD and formation of a stable complex between the protein and the reduced substrate (*4*).

The overall structures of FprA:NADPO and $FprA_{red}$:NADPH are essentially identical, with a rmsd of 0.29 Å for 6894 atoms. However, enzyme reduction is associated to a few differences in the active site. A first observation concerns the flavin conformation. The angle between pyrimidine and dimethylbenzene rings in $FprA_{red}$:NADPH is 7.9°. This value, although small, is twice the corresponding angle observed

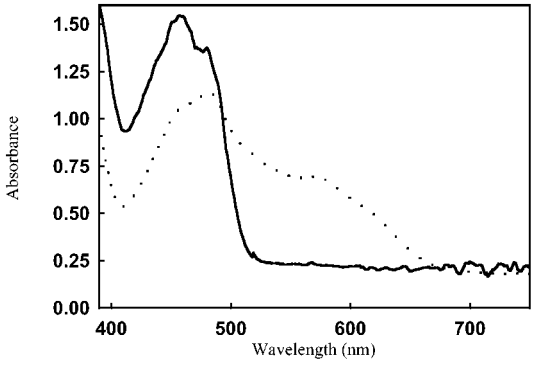

FIGURE 7: Microspectrophotometric analysis of FprA crystals. Polarized absorption spectra were recorded on an oriented crystal with the electric vector of the linearly polarized light parallel to the *a* crystal axis. The spectrum of the oxidized crystal is shown in solid line, while the dashed line is the spectrum recorded on the same crystal after 30 min of soaking in 10 mM NADPH under aerobic conditions.

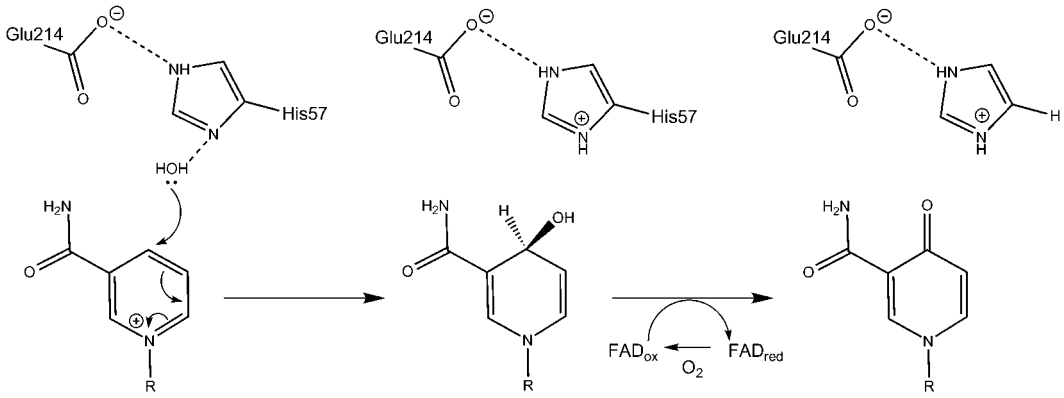

FIGURE 8: Proposed mechanism for $NADP^+$ derivative formation. The water molecule performing the nucleophilic attack is proposed to correspond to water 1, found in the $FprA_{red}$:NADPH structure (see Figure 5b).

in the oxidized enzyme and indicates a slight bent in the reduced cofactor conformation. A more significant difference with respect to FprA:NADPO was found in the NADP ligand. Namely, the additional electron density on the C4 atom was not present in the $FprA_{red}$:NADPH structure (Figure 5b). Rather, a peak of electron density was found in proximity of the C4 atom, but not continuos with its density. This peak was identified as a water molecule, located at 3.39 Å from the C4 atom of NADPH and involved in several bifurcated H-bonds with active site residues. This water molecule has been found in monomer A but not in chain B of $FprA_{red}$:NADPH, although the extra oxygen covalently bound to C4 was absent also in monomer B. This unique water molecule of $FprA_{red}$:NADPH has been named water 1. The absence of the NADP covalent modification does not alter the conformation of the ligand, which is indistinguishable from that found in the oxidized enzyme.

Some interesting differences between FprA:NADPO and $FprA_{red}$:NADPH concern two active site residues, His57 and Glu214. These side chains are positioned above FAD and $NADP^+$ with their side chains H-bonded to each other (Figure 5). In subunit A of the $FprA_{red}$:NADPH structure, these residues display an electron density consistent with a double conformation. In both these alternate conformations, His57 and Glu214 are displaced by about 1 Å away from the nicotinamide ring, relative to the conformation found in FprA:NADPO (Figure 5c). This displacement creates a space that is filled by water 1. In one of the alternate conformations of His57, the Nδ atom is within H-bond distance from this water molecule, while the Nϵ atom is H-bonded to the side chain of Glu214.

The shifted conformations of His57 and Glu214 are not present in subunit B of $FprA_{red}$:NADPH, where they adopt the same conformation present in the oxidized protein. This is likely due to the different crystal contacts. In subunit A, these two active site residues are far from a symmetry related protein molecule. They have the freedom to move and adopt double conformations, allowing water 1 to place itself in the active site. On the contrary, in monomer B, a symmetry-related molecule is in contact with these residues, being at about 4.5 Å from them. Therefore, in monomer B, crystal packing interactions seem to prevent the conformational changes observed in monomer A. However, the presence of unmodified NADPH in both subunits of the $FprA_{red}$:NADPH complex indicates that the exchange of NADPO for NADPH in the crystal lattice can occur.

The relative positioning of the nicotinamide and flavin rings observed in the two FprA complexes is perfectly suited for the hydride transfer reaction thought to underlie the NADPH-dependent oxidation of FAD (*4*). Such a steric relation between the substrate and the cofactor is very similar to that found in the structures of AR and several other NAD(P)H-dependent flavoproteins (*13*, *34*) in which a hydride transfer mechanism is known to occur.

Mechanism of $NADP^+$ Modification. The geometry of the active site observed in the $FprA_{red}$:NADPH structure suggests a possible mechanism for formation of the NADPO compound found in the oxidized enzyme (Figure 8). With reference to monomer A of $FprA_{red}$:NADPH, Glu214, His57, and water 1 appear to form a sort of catalytic triad (*37*). In one of the alternate conformations, the side-chain oxygens of Glu214 are H-bonded to the Nϵ atom of His57, while the Nδ atom of the histidine is within H-bond distance from water 1 (Figure 5b). This geometry is reminiscent of the catalytic triad of serine proteases (*37*), with water 1 fulfilling the role of the serine Oγ atom in proteases. Thus, the interaction of Glu214 with the imidazole group should increase the basicity of His57, which in turn would become more prone to accept a proton from water 1. The final result would be a transient salt bridge between Glu214 and the positively charged His57, and a hydroxyl ion in place of water 1. This ion can carry out a nucleophilic attack on the C4 atom of $NADP^+$, yielding a covalent adduct with a hydroxyl group introduced on the substrate. The subsequent step would be hydride transfer from C4 of the hydroxylated NADPH to N5 of FAD, coupled to proton release from the −C4−OH group of the hydroxylated NADPH. The ultimate result of these reactions is the modified $NADP^+$, as seen in the FprA:NADPO structure.

Several observations support the proposed mechanism. Water 1 lays slightly out of the nicotinamide plane, on the side opposite to that facing the flavin. Thus, the hydroxyl group resulting from the nucleophilic attack by the water would point away from the cofactor. Conversely, the C4-bound hydrogen atom of the hydroxylated NADPH would point toward the flavin, as required for the postulated hydride transfer reaction (Figure 8). Another point is the geometry of the "FprA triad". It is known that in the classical triads the carboxylate−imidazole interaction has usually a favorable geometry, while the H-bond between imidazole and the Ser Oγ is often strained (*37*). This decreases the energy of this bond and favors the proton-relay process. In FprA, this is

actually the observed situation. The interaction between Glu214 and His57 is well in agreement with ideal H-bond geometry, whereas the pair His57−water 1 is interacting through a much more distorted H-bond (distance Nδ−water 1 = 3.28 Å, angle Cβ−Nδ−water 1 = 59°)

For $NADP^+$ modification to occur, the C4 atom of the FprA-bound $NADP^+$ must have an electrophilic character. The neighboring electron-deficient oxidized flavin should exert a polarizing effect on the reactive carbon atom of $NADP^+$, making it more prone to a nucleophilic attack. An additional effect might be due to the cis conformation of the nicotinamide ring, which places the amide nitrogen at 2.65 Å from the extra oxygen atom of NADPO. The presence of this intramolecular H-bond interaction may stabilize the derivative, thus facilitating its formation. The cis conformation of the FprA-bound $NADP^+$ is unusual, since in most NADP-binding proteins, the trans conformation is found (*38*). To our knowledge, the $NADP^+$ derivative of FprA has not been found in other enzyme structures. The crystallographic and mass spectrometry data show that the derivative forms upon incubation of the oxidized protein with $NADP^+$. Whether derivative formation can occur in the cellular environment and whether it has any physiological role are subjects for future studies.

ACKNOWLEDGMENT

The protein crystallography group of the University of Pavia is member of the *Mycobacterium tuberculosis* Structural Genomics Consortium, whose support is gratefully acknowledged. We thank the EMBL/DESY staff for assistance during data collection.

REFERENCES

1. Snider, D. E., Jr., and La Montagne, J. R. (1994) The neglected global tuberculosis problem: a report of the 1992 World Congress on Tuberculosis, *J. Infect. Dis. 169*, 1189−1196.
2. *Mycobacterium tuberculosis* Structural Genomics Consortium (http://www.doe-mbi.ucla.edu/TB, accessed June 2002).
3. Cole, S. T., et al., and Barrell, B. G. (1998) Deciphering the biology of *Mycobacterium tuberculosis* from the complete genome sequence, *Nature 393*, 537−544.
4. Fischer, F., Raimondi, D., Aliverti, A., and Zanetti, G. *Mycobacterium tuberculosis* FprA, a novel bacterial NADPH-ferredoxin reductase, *Eur. J. Biochem*, in press.
5. Schaffer, A. A., Aravind, L., Madden, T. L., Shavirin, S., Spouge, J. L., Wolf, Y. I., Koonin, E. V., and Altschul, S. F. (2001) Improving the accuracy of PSI−BLAST protein database searches with composition-based statistics and other refinements, *Nucleic Acids Res. 29*, 2994−3005.
6. Li, J., Saxenan, S., Pain, D., and Dancis, A. (2001) Adrenodoxin reductase homolog (Arh1p) of yeast mitochondria required for iron homeostasis, *J. Biol. Chem. 276*, 1503−1509.
7. Manzella, L., Barros, M. H., and Nobrega, F. G. (1998) ARH1 of *Saccharomyces cerevisiae*: a new essential gene that codes for a protein homologous to the human adrenodoxin reductase, *Yeast 14*, 839−846.
8. Lambeth, J. D., Seybert, D. W., Lancaster, J. R., Jr., Salerno, J. C., and Kamin, H. (1982) Steroidogenic electron transport in adrenal cortex mitochondria, *Mol. Cell. Biochem. 45*, 13−31.
9. Grinberg, A. V., Hannemann, F., Schiffler, B., Muller, J., Heinemann, U., and Bernhardt, R. (2000) Adrenodoxin: structure, stability, and electron-transfer properties, *Proteins 40*, 590−612.
10. Bernhardt, R. (1996) Cytochrome P450: structure, function, and generation of reactive oxygen species, *Rev. Physiol. Biochem. Pharmacol. 127*, 137−221.
11. De Voss, J. J., Rutter, K., Schroeder, B. G., and Barry, C. E., III (1999) Iron acquisition and metabolism by mycobacteria, *J. Bacteriol. 181*, 4443−4451.
12. Ziegler, G. A., Vonrhein, C., Hanukoglu, I., and Schulz, G. E. (1999) The structure of adrenodoxin reductase of mitochondrial P450 systems: electron transfer for steroid biosynthesis, *J. Mol. Biol. 289*, 981−990.
13. Ziegler, G. A., and Schulz, G. E. (2000) Crystal structures of adrenodoxin reductase in complex with $NADP^+$ and NADPH suggesting a mechanism for the electron transfer of an enzyme family, *Biochemistry 39*, 10986−10995.
14. Muller, J. J., Lapko, A., Bourenkov, G., Ruckpaul, K., and Heinemann, U. (2001) Adrenodoxin reductase-adrenodoxin complex structure suggests electron-transfer path in steroid biosynthesis, *J. Biol. Chem. 276*, 2786−2789.
15. Mozzarelli, A., and Rossi, G. L. (1996) Protein function in the crystal, *Annu. Rev. Biophys. Biomol. Struct. 25*, 343−365.
16. Leslie A. G. (1999) Integration of macromolecular diffraction data, *Acta Crystallogr., Sect. D 55*, 1696−1702.
17. Collaborative Computational Project Number 4 (1994) The CCP4 suite: programs for protein crystallography, *Acta Crystallogr., Sect. D 50*, 760−767.
18. Read, R. J. (2001) Pushing the boundaries of molecular replacement with maximum likelihood, *Acta Crystallogr., Sect. D 57*, 1373−1382.
19. Cowtan, K., and Main, P. (1998) Miscellaneous algorithms for density modification, *Acta Crystallogr., Sect. D 54*, 487−593.
20. Perrakis, A., Morris, R., and Lamzin, V. S. (1999) Automated protein model building combined with iterative structure, *Nat. Struct. Biol. 5*, 458−463.
21. Perrakis, A., Harkiolaki, M., Wilson, K. S., and Lamzin, V. S. (2001) ARP/wARP and molecular replacement, *Acta Crystallogr., Sect. D 57*, 1445−1450.
22. Murshudov, G. N., Vagin, A. A., and Dodson, E. J. (1997) Refinement of macromolecular structures by the maximum-likelihood method, *Acta Crystallogr., Sect. D 53*, 240−255.
23. Jones, T. A., Zou, J. Y., Cowan, S. W., and Kjeldgaard, M. (1991) Improved methods for building models in electron density maps and the location of errors in these models, *Acta Crystallogr., Sect. A 47*, 110−119.
24. Laskowski, R. A., MacArthur, M. W., Moss, D. S., and Thornton, J. M. (1993) PROCHECK: a program to check the sterochemistry of protein structures. *J. Appl. Crystallogr. 26*, 283−291.
25. Kleywegt, G. J., Zou, J. Y., Kjeldgaard, M., and Jones, T. A. (2001). Around O, in *International Tables for Crystallography, Vol. F, Crystallography of Biological Macromolecules* (Rossmann, M. G., and Arnold, E., Eds.) Chapter 17.1, pp 353−356 and 366−367, Kluwer Academic Publishers, Dordrecht, The Netherlands.
26. Kraulis, P. J. (1991) MOLSCRIPT: a program to produce both detailed and schematic plots of protein structures, *J. Appl. Crystallogr. 24*, 946−950.
27. Esnouf, R. M. (1999) Further additions to MolScript version 1.4, including reading and contouring of electron-density maps, *Acta Crystallogr., Sect. D 55*, 938−940.
28. Wallace, A. C., Laskowski, R. A., and Thornton, J. M. (1995) LIGPLOT: a program to generate schematic diagrams of protein-ligand interactions, *Protein Eng. 8*, 127−134.
29. Tahallah, N., Pinkse, M., Maier, C. S., and Heck, A. J. (2001) The effect of the source pressure on the abundance of ions of noncovalent protein assemblies in an electrospray ionization orthogonal time-of-flight instrument, *Rapid Commun. Mass Spectrom. 15*, 596−601.
30. Dym, O., and Eisenberg, D. (2001) Sequence-structure analysis of FAD-containing proteins, *Protein Sci. 10*, 1712−1728.
31. Vallon, O. (2000) New sequence motifs in flavoproteins: evidence for common ancestry and tools to predict structure, *Proteins 38*, 95−114.
32. Schulz, G. E. (1992) Binding of nucleotides by proteins, *Curr. Opin. Struct. Biol. 2*, 61−67.
33. Wierenga, R. K., Drenth, J., and Schulz, G. E. (1983) Comparison of the three-dimensional protein and nucleotide structure of the FAD-binding domain of *p*-hydroxybenzoate hydroxylase with the FAD- as well as NADPH-binding domains of glutathione reductase, *J. Mol. Biol. 167*, 725−739.
34. Fraaije, M. W., and Mattevi, A. (2000) Flavoenzymes: diverse catalysts with recurrent features, *Trends Biochem. Sci. 25*, 126−132.
35. Almarsson, O., and Bruice, T. C. (1993) Evaluation of the factors influencing reactivity and stereospecificity in NAD(P)H dependent dehydrogenase enzymes, *J. Am. Chem. Soc. 115*, 2125−2138.

36. Van Berkel, W. J., van den Heuvel, R. H., Versluis, C., and Heck, A. J. R. (2000) Detection of intact megaDalton protein assemblies of vanillyl-alcohol oxidase by mass spectrometry, *Protein Sci. 9*, 435−439.
37. Dodson, G., and Wlodawer. A. (1998) Catalytic triads and their relatives, *Trends Biochem. Sci. 23*, 347−352.
38. Carugo, O., and Argos, P. (1997) NADP-dependent enzymes. I: Conserved stereochemistry of cofactor binding, *Proteins 28*, 10−28.
39. Berman, H. M., Westbrook, J., Feng, Z., Gilliland, G., Bhat, T. N., Weissig, H., Shindyalov, I. N., and Bourne, P. E. (2000) The Protein Data Bank, *Nucleic Acids Res. 28*, 235−242.
40. Thompson, J. D., Higgins, D. G., and Gibson, T. J. (1994) CLUSTAL W: improving the sensitivity of progressive multiple sequence alignment through sequence weighting, position-specific gap penalties and weight matrix choice, *Nucleic Acids Res. 22*, 4673−4680.

BI025858A